Electrospun polymer of intrinsic microporosity fibers and their use in the adsorption of contaminants from a nonaqueous system

Caili Zhang, Pei Li, Bing Cao

College of Materials Science and Engineering, Beijing University of Chemical Technology, Chaoyang District North Third Ring Road 15, Beijing 100029, China
Correspondence to: P. Li (E-mail: lipei@mail.buct.edu.cn) and B. Cao (E-mail: bcao@mail.buct.edu.cn)

ABSTRACT: The smooth and uniform polymer of intrinsic microporosity (PIM-1) fibers, which have high adsorption capacities toward organic contaminants from nonaqueous systems, were successfully obtained by electrospinning. According to the N_2 adsorption–desorption analysis, the surface area of the PIM-1 fibers was higher than that of the PIM-1 powder. The higher surface area of the fibers did not come from the interfiber pores but from intrafiber pores formed by the fast evaporation of the solvent in the electrospinning process. The PIM-1 fibers had more mesopores than the PIM-1 films. As a result, the adsorption rates of the dyes on the fibers were much higher than those on the dense films. We found that the adsorption data fitted perfectly with the pseudo-second-order model and intraparticle diffusion model. The adsorption mechanism between the dyes and PIM-1 was π–π interaction. Therefore, the dye could be desorbed from PIM-1 with toluene; this was a better π-electron-rich donor than the dye. In summary, we believe that the use of PIM-1 fibers for organic solvent recovery is a green, sustainable, and efficient method, and they have a great potential for industrial applications. © 2016 Wiley Periodicals, Inc. J. Appl. Polym. Sci. **2016**, *133*, 43475.

INTRODUCTION

With the rapid expansion of various industries, organic solvents are used extensively in numerous manufacturing processes; these include the petrochemical, food, painting, and pharmaceutical industries. Along with the use of huge volumes of organic solvents, it is imperative to control solvent discharge and recover used solvents to diminish air and water pollution and also reduce solvent costs.[1,2]

A typical technique used for organic solvent recovery is distillation. This process usually involves the utilization of high energy and operation costs.[3] Recently, an alternate approach to the use of polymeric membranes, referred to as *organic solvent nanofiltration (OSN)*, can in many cases reduce these costs effectively.[4,5] OSN is an emerging membrane-based separation process; it is used for organic solvent recovery and has already shown great potential in terms of savings and applicability to industrial processes.[6,7] The membrane materials for OSN are required to not only offer high-filtration performance (solvent permeability/retention) but also show high chemical and mechanical stability, whereas these practical requirements limit a large amount of polymers to be used for OSN.

Previously, it has been shown that glassy polymers with a high fraction of free volume, such as poly(1-trimethylsilyl-1-propyne) and polymer of intrinsic microporosity (PIM-1), are prospective membrane materials for OSN.[8,9] Because of the good mechanical properties and the rigid nature of their macromolecular chains, a porous structure with free volume elements of about a 1-nm size is naturally formed during the casting of the polymeric solution.

Unfortunately, some solutes in organic solvents cannot be separated by membranes because of negative retention because of the greater affinity of solute molecules to membrane materials, such as PIM-1 and poly(1-trimethylsilyl-1-propyne), rather than the interaction of solute and membrane with organic solvent.[10–13] The negative retention solutes are often nonaqueous dyes; these are widely used in various industrial sectors, such as the coloration of cellulose esters, celluloid, poly(vinyl acetates), oil, and plastics.[14,15] During these processes, a large amount of dye-contaminated organic solvent is generated. Because of the high affinity of these dyes to high-free-volume polymers, we proposed an adsorption approach to remove them from organic solvents with adsorbent made of PIM-1.

Adsorption is one of the most effective processes that industries use to reduce hazardous inorganic/organic pollutants present in the effluent.[16] The application of adsorption in the removal of contaminants from aqueous solution is widely used, but very few reports can be found for the removal of contaminants from organic solvents. The selection of adsorbent material is especially important for adsorption technology. However, many traditional adsorbents, for instance, activated carbon, mesoporous silica, and metal–organic frameworks, are hydrophilic; these cannot be used in organic solvents. To be used in organic systems, first, the adsorbent should be hydrophobic. Therefore, it is of great important for the development of efficient adsorbents with large adsorption capacities, good flexibility, recyclability, and stability in organic solvents. A suitable adsorbent should have not only a rapid and effective adsorption ability but also a large capacity and good regenerability to the pollutants.

PIM-1 is a hydrophobic polymer that has not only the high internal surface area of conventional microporous materials, such as zeolites or activated carbons, but also the processability of polymers.[17] Among the various technologies available for the preparation of a porous adsorbent, electrospinning, as a very simple and versatile way, has been used extensively to produce three-dimensional porous membranes for various applications.[18,19] The obtained fibrous membranes exhibited many outstanding characteristics, such as a high porosity, large surface-area-to-volume ratio, and excellent flexibility; this makes them ideal candidates for adsorbents.[20] In our previous work, we introduced the possibility of using PIM-1 fibers to adsorb dyes from hexane for organic solvent recovery.[21]

In this study, smooth and uniform PIM-1 fibers, which have high adsorption capacities toward organic contaminants from a nonaqueous system, were successfully fabricated with electrospinning. The difference between the surface area and pore volume between the PIM-1 powder and PIM-1 fibers were investigated. The adsorptions of Solvent Blue 35 and Oil Red O into the PIM-1 dense film and PIM-1 fibers were examined to explore the influence of the mesopores on the adsorption rate. The adsorption mechanism between the dyes and PIM-1 through host–guest interaction was also studied.

EXPERIMENTAL

Materials
5,5′,6,6′-Tetrahydroxy-3,3,3′,3′-tetramethyl-1,1′-spirobisindane (TTSBI; 97%) was purchased from Alfa Aesar. 2,3,5,6-Tetrafluoroterephthalonitrile (TFTPN; 99%), potassium carbonate (K$_2$CO$_3$; > 99.5%), and anhydrous N,N'-dimethylformamide were purchased from Sigma-Aldrich. Hydrochloric acid (37.5%), anhydrous ethanol, and toluene were obtained from Tianjin Fu Chen Chemical Reagents Factory. 1,1,2,2-Tetrachloroethane (>99.9%), Solvent Blue 35(>99%), and Oil Red O (>99%) were purchased from J&K Co., Ltd. TTSBI was purified by recrystallization in methanol, whereas TFTPN was sublimated *in vacuo*. Other chemicals were used as received.

PIM-1 Synthesis
PIM-1 was synthesized via a nucleophilic substitution reaction between TTSBI and TFTPN with K$_2$CO$_3$ as the catalyst in an NMP solution. The detailed synthesis procedure was reported elsewhere.[22] We obtained the PIM-1 polymer in powder form with a molecular weight of 292,000 g/mol by carrying out the reaction for 3 days under a nitrogen blanket.

Dense Film Preparation
The PIM-1 dense films were prepared with the solution casting method. The PIM-1 powder was dissolved in chloroform at a concentration of 2 wt %. The PIM-1 solution was filtered with a 0.45-μm polypropylene membrane and then cast into a stainless steel ring, which was placed on a glass board and covered by another glass board to reduce the rate of solvent evaporation. The dense film was formed after 3 days. After that, the film, with a thicknesses of 50 ± 5 μm, was peeled off from the glass board and placed in a vacuum oven at 70 °C overnight to remove the trace amount of residual solvent.
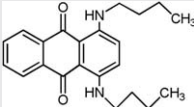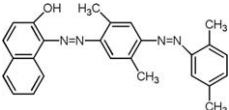
Electrospinning
The PIM-1 powder was dissolved in 1,1,2,2-tetrachloroethane at concentrations ranging from 7 to 10 wt %. The PIM-1 solutions were megastirred at 80 °C for 5 h and cooled down to room temperature (RT) and then degassed *in vacuo*. After that, about 7 mL of the PIM-1 solution was placed in a 10-mL syringe, which was equipped with a blunt metal needle with an inner diameter of 0.37 mm. A syringe pump was used to maintain an injection rate of 0.01 mL/min. A grounded drum covered by a piece of aluminum foil was used as the fiber collector. The drum rotation speed was controlled at 100 rpm. The distance from the needle tip to the collector and the voltage were set at 17 cm and 10–12 kV, respectively. The fibers electrospun from different solutions with the PIM-1 concentrations of 7, 8, 9, and 10 wt % were coded as F7, F8, F9, and F10, respectively.

Characterization
The molecular weight of PIM-1 was measured by a Waters 515-2410 gel permeation chromatograph, which was calibrated with polystyrene standard samples with a HSPgel RT column. The fiber morphologies were investigated with field emission scanning electron microscopy (FESEM; Hitachi S-4700). The nitrogen adsorption and desorption isotherms were measured at 77 K with a Quantachrome Autosorb-1 (Quantachrome Instruments, Boynton Beach, FL). All of the samples were degassed at 150 °C for at least 12 h before the sorption measurements. The specific surface areas and pore size distributions were calculated on the basis of the data from the adsorption isotherms with the Brunauer–Emmett–Teller (BET) and nonlocal density functional theoretical models, respectively. Mercury intrusion porosimetry was performed with a PoreMaster-60 GT from Quantachrome Instruments. The pore size distribution (the interfibers pores) and cumulative surface area were calculated from the mercury intrusion data through the application of the Washburn equation. Ultraviolet–visible (UV–vis) spectra were recorded on a Shimadzu spectrophotometer (UV-1700, Japan). The density of the fibrous membrane was measured at 25 °C with a precision electronic balance equipped with a density determination kit (Shanghai, China). Specifically, the sample was weighed in air and in hexane. The density was calculated directly according to eq. (1):[23]

Table I. Molecular Structures and Characteristic Properties of the Dyes Used in This Study[12]

Dye	M_w (Da)	Structure	λ_{max} (nm)	δ (MPa$^{0.5}$)	V_{calc} (Å^3)
Solvent Blue 35	350 (neutral)		644	23.7	685
Oil Red O	408 (neutral)		517	25.2	820

λ_{max}, maximum wavelength; M_w, weight-average molecular weight; V_{calc}, the calculated volume.

$$D_s = \frac{A}{A-B}(D_0 - D_L) + D_L \qquad (1)$$

where D_s is the density of the sample, A is the weight of the sample in air, B is the weight of the sample in hexane, D_0 is the density of hexane at the exactly measured temperature, and D_L is the air density (0.0012 g/cm^3).

Adsorption Measurements

Table I lists the molecular volumes, weights, and structures of Solvent Blue 35 and Oil Red O, which were used as adsorbates in this study. Before the adsorption measurements, the electrospun fibers and dense films were immersed in methanol for 4 h at ambient temperature and were subsequently dried *in vacuo* at 100 °C overnight to ensure a similar thermal history. To determine the adsorption rate, 10-mg fibers or dense film samples were immersed in glass vials containing 20 mL of ethanol solution of which the concentrations of dyes were kept at 10 and 40 mg/L, respectively. The solutions were stirred by a magnetic rotor at RT. After a predetermined time interval, the dye concentration of the ethanol solution was determined by a UV–vis spectrophotometer. The amount of adsorbed dye was calculated with eq. (2):

$$q_t = \frac{(C_0 - C_t) V}{m} \qquad (2)$$

where C_0 is the initial concentration, C_t is the residual concentration at time t, V is the volume of the solution, and m is the mass of the adsorbent. So, a curve of the adsorbed dye amount versus time was generated to calculate the adsorption rate.

RESULTS AND DISCUSSION

Characterization of PIM-1 Electrospun Microfibers

In the electrospinning process, a jet of polymer fluid is charged by a high-voltage power supply. As the voltage increases, the shape of the pendant droplet at the end of the capillary tip changes from a hemisphere to a cone; this is called the Taylor cone.[24] If the applied voltage reaches a critical value, the charged jet starts to spin toward the collector. Usually, the collected sample exhibits three typical morphologies, that is, bead, bead-on-string, and fiber structures.[25] The reason is that the surface tension of the polymer solution intends to change the shape of the jet into sphere to reduce the surface area, whereas the viscoelastic force resists rapid changes in the jet shape.[25–27]

Increasing the polymer concentration makes the solution viscosity higher and the surface tension lower so that the shapes of the beads gradually change from spherical to spindlelike. When the PIM-1 concentration is lower than 7 wt %, only PIM-1 beads can be obtained. As the PIM-1 concentrations increase to 7, 8, or 9 wt %, the bead-on-string morphologies are formed, as shown in Figure 1(a–c). The average distance between adjacent beads and fiber diameters both increase, and the shapes of the beads change from spherical to spindlelike. When the PIM-1 concentration increased to 10 wt %, the bead structure disappeared and smooth fibers were obtained, as shown in Figure 1(d). As the PIM-1 concentration increased further, the fiber was still smooth with increased diameter. Figure 2(a) shows the higher magnification FESEM image of F10; it was smooth and uniform with an average fiber diameter of about 1.7 μm, as reported in ref. 28. Both scanning electron microscopy and transmission electron microscopy images demonstrate that the obtained fibers were smooth and uniform. (The different magnifications of the transmission electron microscopy images for F10 are shown in Figure S1 in the Supporting Information.)

Figure 3(a) shows the nitrogen adsorption–desorption isotherms of the F10 and PIM-1 powder, whereas the BET surface area and pore size distribution of the PIM-1 dense film could not be characterized by the N$_2$ adsorption–desorption method. As shown in Figure S2 (Supporting Information), no significant uptake was observed at low pressures, but at a certain point, a strong uptake took place. Such a phenomenon indicated the complicated molecular interactions at low temperature (77 K), and although it has been reported in other works,[29–31] it was not well understood for the PIM-1 dense film and other high free-volume polymers. So, we just made a comparison of N$_2$ sorption isotherms between the PIM-1 fiber and PIM-1 powder. Both samples showed hysteresis loops (the desorption curve was above the adsorption curve), and the hysteresis started from very low relative pressures; this indicated that both samples consisted of micropores and mesopores. This phenomenon is often observed for microporous material.[32] The BET specific surface areas of the F10 and PIM-1 powder were 1114 and 976 m^2/g, respectively; these were comparable to the reported data of PIM-1.[17,33] It is well know that the microporosity of PIM-1 arises from its contorted shape and extreme rigidity; these inhibit the efficient packing of the macromolecules in the
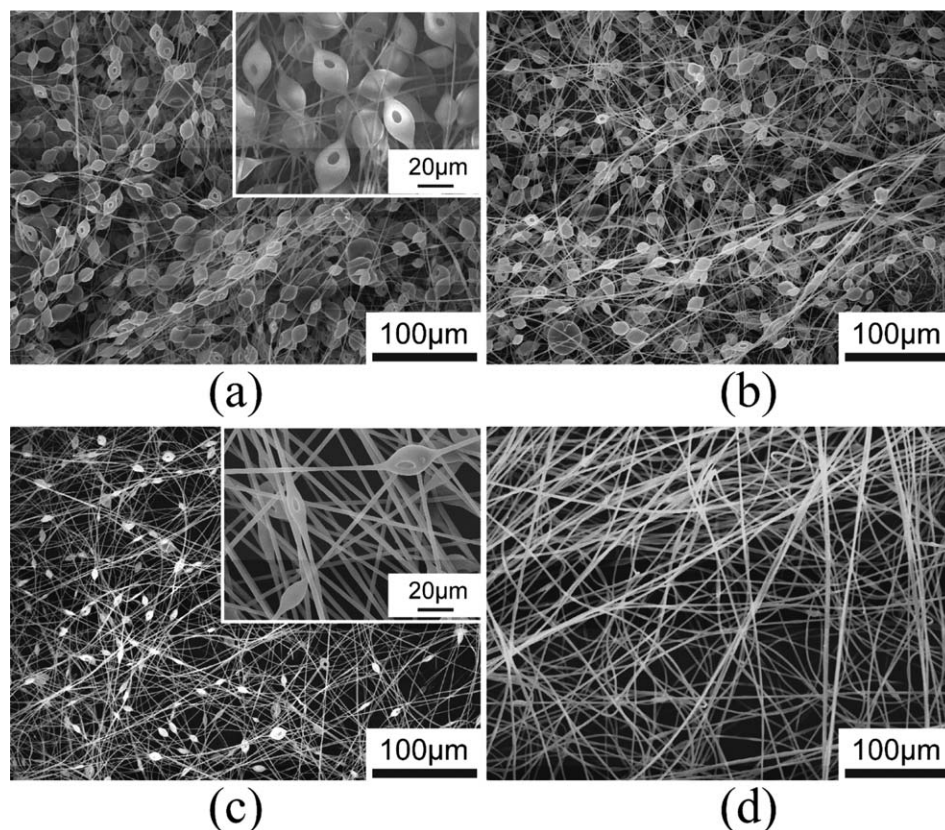
Figure 1. FESEM images of PIM-1 fibers electrospun from solutions with various PIM-1 concentrations: (a) F7, (b) F8, (c) F9, and (d) F10.

solid state. The spirocenters induce the randomly contorted shape, and the rigid fused-ring structure ensures that the relaxation of the porous structure by bond rotation is prohibited. This microporosity is intrinsic to the polymer's molecular structure and is not dependent on the history of the material. Thus, the microporosity can be described as intrinsic. In contrast to its microporosity, the mesoporosity demonstrated by PIM-1 is dependent on the form of the material. Figure 3(b,c) are the data of pore size distribution and cumulative pore volume of the F10 and PIM-1 powder. Compared with F10, the PIM-1 powder had more micropores and less pore volume. This observation was also proven by the data listed in Table II, in which

the average pore width, total pore volume, and mesopore volume of F10 were all higher than those of the PIM-1 powder. The reason why the surface area and mesopore volume of F10 were higher than those of the powder are discussed later.

It is well known that two types of pores exist in electrospun fibrous membranes, that is, interfiber and intrafiber pores.[34] Interfiber pores are formed by fiber crossing, whereas intrafiber pores refer to the pores existing inside the fibers. According to Table II, the BET surface area of F10 was much greater than that of the PIM-1 powder. We attributed to the increases in the surface areas of both interfiber pores and intrafiber pores. The surface area of the interfiber pores was similar to the total area
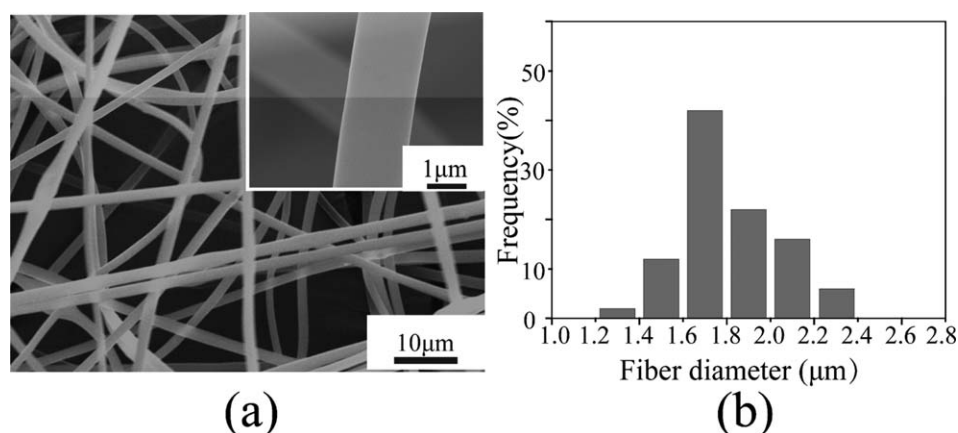

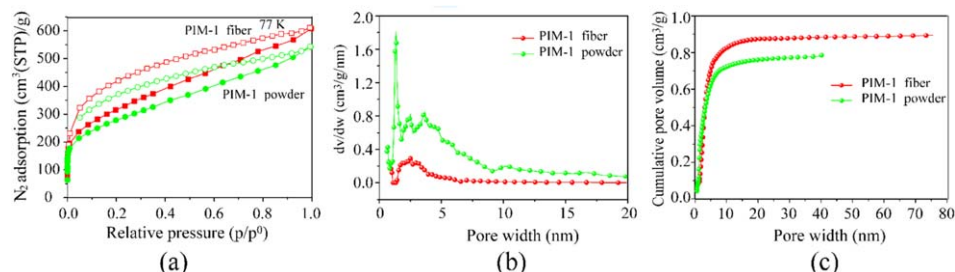**Figure 2.** (a) FESEM images of F10 and (b) fiber diameter distribution.

Figure 3. (a) N$_2$ adsorption–desorption isotherms (solid symbols represent adsorption data, and empty symbols represent desorption data), (b) nonlocal density functional theoretical pore volume distributions, and (c) cumulative pore volume of the PIM-1 powder and F10. [Color figure can be viewed in the online issue, which is available at wileyonlinelibrary.com.]

of the fiber surface. To estimate the fiber surface area, the fiber was assumed to have infinite length. Equation (3) was applied to calculate the surface area of a single fiber[35]:

$$S_S = \pi D l + 2\pi \left(\frac{D}{2}\right)^2 \qquad (3)$$

where S_S is the surface area of a single electrospun fiber, l is the length of the fiber, and D is the diameter of the fiber (μm). The specific volume and the volume of a single fiber were estimated with eqs. (4) and (5):

$$V_0 = \frac{1}{\rho} \qquad (4)$$

$$V_S = \pi \left(\frac{D}{2}\right)^2 l \qquad (5)$$

where V_0 is the specific volume of the PIM-1 fiber (cm^3/g), ρ is the fiber density (g/cm^3), and V_S is the volume of a single fiber (cm^3). In a combination of eqs. (3–5), the surface area of 1 g of fiber sample was calculated with eq. (6):

$$S_t = \frac{4}{\rho D} + \frac{2}{\rho l} \qquad (6)$$

where S_t is the theoretical surface area of the fibers (m^2/g). Because the value of l was assumed to be infinite, we obtained eq. (7) by ignoring $2/(\rho l)$:

$$S_t = \frac{4}{\rho D} \qquad (7)$$

The density of the electrospun fibers tested in our laboratory was 1.09 g/cm^3; this was similar to the density of the PIM-1 powder,[36] and the relationship between the estimated surface area of the fibers and the fiber diameter is shown in Figure 4(a). The fiber surface area increased slightly from 1.6 to

2.8 m^2/g through a decrease in the fiber diameter from 2.3 to 1.3 μm. Thus, the fiber surface area was insensitive to the change in the fiber diameter in the micrometer range. The mercury intrusion porosimetry measurement was also performed to directly determine the interfiber pore surface area. As shown in Figure 4(b,c), the cumulative surface area of F10 approached 8 m^2/g as the mercury entered the smallest pores with a diameter of 6 nm. The pressure of mercury was several megapascals under these conditions. The high pressure led to the severe deformation of the fiber sample. Therefore, the data obtained at high pressures did not represent the real interfiber pore surface area. Because both the calculated and measured interfiber pore surface areas of the electrospun fibers were less than 10 m^2/g, the much higher surface areas of the PIM-1 fibers came from their high intrafiber pore surface areas, which resulted from the chain entanglements and rapid evaporation of solvent during the electrospinning process.[37]

Adsorption Rate

Figure 5 shows the sorption curves of Solvent Blue 35 and Oil Red O on both PIM-1 dense films and electrospun fibers at two different dye concentrations of 10 and 40 mg/L, respectively. Apparently, the rates of adsorption on the fiber samples were much faster than those on the dense film samples. Specifically, 95% adsorption equilibrium on the fiber samples was achieved in less than 20 min, whereas on the dense film samples, it took more than 200 min to reach 60–70% sorption equilibrium, and the whole adsorption process lasted for 6000 min.

The reason for the faster adsorption rates on the PIM-1 fibers was that there were more mesopores in the fibers than in the dense films. According to Jeromenok and Weber's[38] definition, there exists open and restricted micropores in amorphous microporous polymers. During the electrospinning process, the solvent evaporated quickly, and it prevented the rearrangements of the polymer chains into equilibrium packing configurations. However, in the film-casting process, the polymer chains had more time to rotate and pack. This resulted in a denser packing of the polymer chains. Therefore, the electrospun PIM-1 fibers had more surface areas and mesopores than the PIM-1 dense films. With the existence of more mesopores in the PIM-1 fiber, the path length of the micropores for the diffusion from the mesopores to the interior was shorter than that when the diffusion came directly from the bulk phase to the interior without the aid of mesopores. Under this circumstance, the mesopores

Table II. Surface Area and Pore Size Analysis Data from N$_2$ Sorption Isotherms of F10 and PIM-1 Powder

	S_{BET} (m^2/g)	DFT average pore width (nm)	DFT TPV (cm^3/g)	V_{meso} (cm^3/g)	V_{micro} (cm^3/g)
F10	1114	2.583	0.894	0.699	0.195
Powder	976	1.326	0.785	0.440	0.345

SBET, the Brunauer-Emmett-Teller (BET) specific surface area; V$_{meso}$, the mesopores volume; V$_{micro}$, the micropores volume.
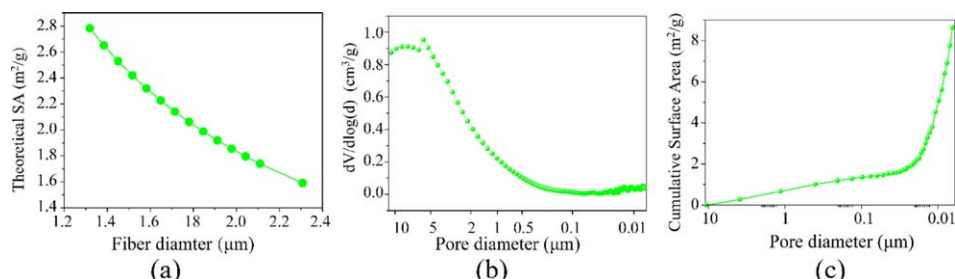
Figure 4. (a) Estimated surface area (SA) of the electrospun PIM-1 fibers as a function of the fiber diameters, (b) pore size distribution of F10, and (c) cumulative surface area of the fibers from the mercury intrusion curve. dv/d log(d), pore volume. [Color figure can be viewed in the online issue, which is available at wileyonlinelibrary.com.]

played a role in not only accelerating the diffusion into micropores but also in increasing the equilibrium coverage of the micropore surface. So, the existence of mesopores enabled the adsorbates to obtain access to the inner and narrow micropores. The equilibrium adsorption capacities of the film samples were lower than those of the fiber samples because the greater number of mesopores existing in the fiber. The adsorption capacity of PIM-1 in the nonaqueous system was comparable to those of other adsorbents used in the aqueous system, especially at low solute concentrations.[16,39]

Adsorption Kinetics
The pseudo-first-order and pseudo-second-order kinetic models,[40,41] which are given in eqs. (8) and (9), were applied to describe the adsorption processes in this study:

$$\log(q_e - q_t) = \log q_e - \frac{k_1 t}{2.303} \tag{8}$$

$$\frac{t}{q_t} = \frac{1}{K_2 q_e^2} + \frac{t}{q_e} \tag{9}$$

where q_e and q_t (mg/g) are the amounts of dye adsorbed at equilibrium and at time t (min), respectively, and k_1 (min^{-1}) and k_2 (g mg^{-1} min^{-1}) are the pseudo-first-order and pseudo-second-order rate constants, respectively. The kinetic parameters and the correlation coefficients (R^2s) were determined by linear regression (Figure 6). As summarized in Table III, the calculated equilibrium adsorption capacities ($q_{e,\mathrm{exp}}$) with the pseudo-first-order model did not fit the experimental results ($q_{e,\mathrm{cal}}$), and the R^2s were very low. Hence, the adsorption behaviors did not obey the pseudo-first-order model. In contrast, the simulated
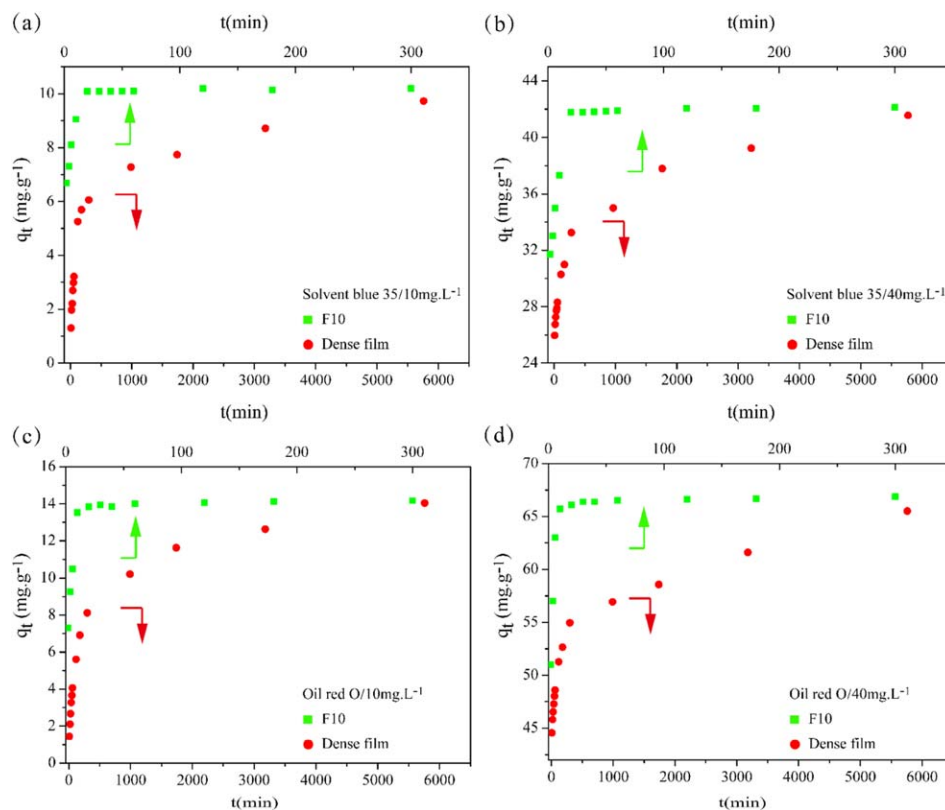

Figure 5. Adsorption rates of the two dyes on the electrospun fibers and dense films at (a) 10 and (b) 40 mg/L for Solvent Blue 35 and (c) 10 and (d) 40 mg/L for Oil Red O. [Color figure can be viewed in the online issue, which is available at wileyonlinelibrary.com.]
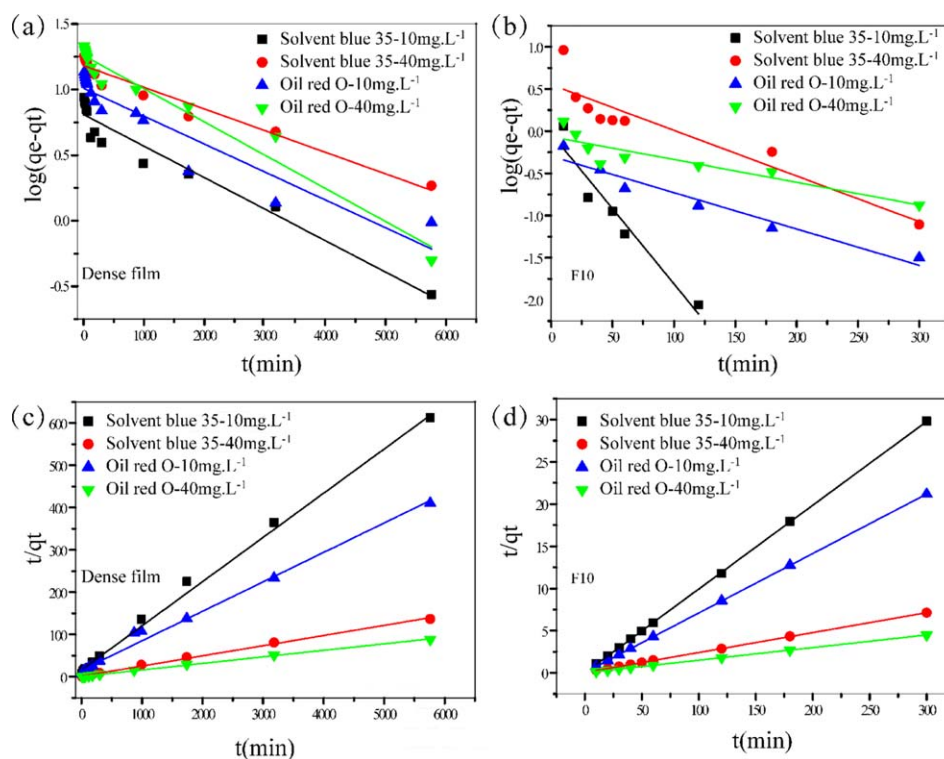
Figure 6. (a,b) Pseudo-first-order and (c,d) pseudo-second-order kinetic plots of adsorption. [Color figure can be viewed in the online issue, which is available at wileyonlinelibrary.com.]

kinetic adsorption curves based on the pseudo-second-order model showed a good fit to all of the experimental data with high R^2s ($R^2 > 0.99$). The values of $q_{e,cal}$ also matched the experimentally determined values of $q_{e,exp}$. This indicated that the kinetic adsorption processes in both the fiber and film samples were well described with the pseudo-second-order model.

Adsorption Mechanism
Intraparticle Diffusion. The adsorption processes of the dyes on the PIM-1 samples could be divided into the following three steps: (1) diffusion of the dye through the boundary layer, (2) intraparticle diffusion, and (3) adsorption of the dye on the sor-

bent surface.[42,43] Because the uptake of the dye at the active sites is a rapid process, the rate limit of adsorption was mainly governed by the rate of liquid phase mass transfer and/or intraparticle mass transfer.[44] Furthermore, the adsorbate species were most probably transported from the bulk of the solution into the solid phase through the intraparticle diffusion process; this is often the rate-limiting step in many adsorption process.[42]

Weber and Morris[45] stated that when intraparticle diffusion is the rate-controlling step, the uptake of the adsorbate linearly increases with the square root of time. Thus, the intraparticle diffusion rate of adsorption (k_i) was estimated through the

Table III. Kinetic Parameters for the Adsorption of Solvent Blue 35 and Oil Red O on the Dense Film and Electrospun Fibers

|	C_0 (mg/L)	$q_{e,exp}$ (mg/g)	Pseudo-first-order model			Pseudo-second-order model		
			k_1 (min^{-1})	$q_{e,cal}$ (mg/g)	R^2	k_2 (g mg^{-1} min)	$q_{e,cal}$ (mg/g)	R^2
Dense film								
Solvent Blue 35	10	9.726	5.29×10^{-4}	6.439	0.941	6.91×10^{-4}	9.562	0.994
	40	41.548	3.63×10^{-4}	15.211	0.953	4.02×10^{-4}	41.631	0.997
Oil Red O	10	14.030	4.68×10^{-4}	10.225	0.874	3.15×10^{-4}	14.351	0.989
	40	65.501	5.58×10^{-4}	18.186	0.957	3.01×10^{-4}	65.724	0.988
Electrospun fibers								
Solvent Blue 35	10	10.192	3.92×10^{-2}	0.933	0.915	0.784	10.075	0.999
	40	42.122	1.19×10^{-2}	3.557	0.840	0.012	42.337	0.999
Oil Red O	10	14.168	9.49×10^{-3}	0.503	0.933	0.098	14.192	0.999
	40	66.867	5.95×10^{-3}	0.858	0.794	0.053	66.889	1
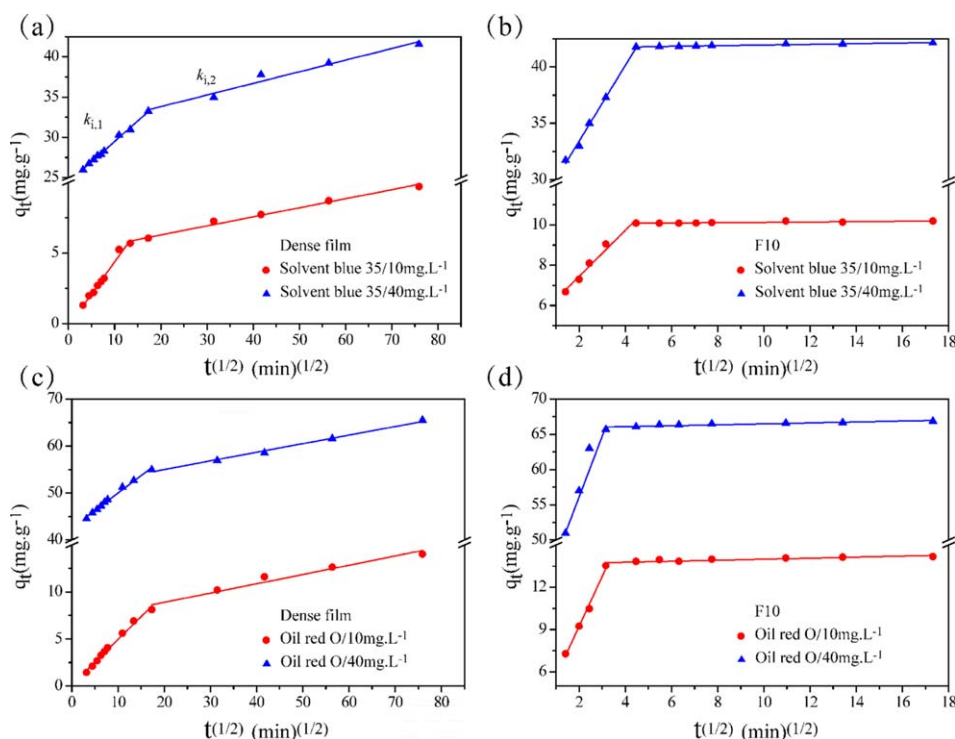
Figure 7. Intraparticle diffusion plots for (a,b) Solvent Blue 35 and (c,d) Oil Red O. $t^{(1/2)}$ represents the time required for the PIM-1 to uptake half of the amount adsorbed at equilibrium. [Color figure can be viewed in the online issue, which is available at wileyonlinelibrary.com.]

calculation of the slope of the amount of adsorbed material per unit mass of adsorbent as a function of the square root of time and can be expressed by eq. (10)[46]:

$$q_t = k_i(t)^{1/2} + C \qquad (10)$$

where k_i is the intraparticle diffusion rate parameter. According to eq. (10), a plot of q_t versus $t^{0.5}$ (where $t^{0.5}$ is the square root of time) should be a straight line with a slope (k_i) and an intercept (C) when the adsorption mechanism followed the intraparticle diffusion model. In this study, two linear sections in the root time plots were evaluated separately with eq. (10), and the model parameters are listed in Table IV. As shown in Figure 7, the plots of q_t against $t^{0.5}$ consisted of two linear sections with different slopes. A similar multilinearity was observed in some aqueous systems, for example, for the dye sorption on sepiolite[43] and peat resin particles.[47] The formation of two linear sections indicated that two types of intraparticle diffusions occurred in the sorption process. The first straight portion was attributed to the macrospore and mesopore diffusions, and the second linear portion stemmed from micropore diffusion.[43,47,48] According to Simons,[49,50] the structure of a porous adsorbent can be described by a pore tree structure. A feature of this description was that the adsorbent materials possessed cylindrical pores whose branching sequence was depicted as a tree or river system. Larger diameter macrospores and mesopores extended into the adsorbent body branching into transitional pores and into micropores. The adsorbate had to diffuse through the larger tree trunk and the lager branches to reach the total surface area within the adsorbent. The net adsorptive rate was limited by the kinetic rate acting at the external surface

or by diffusion through the trunk and branches of the tree. Therefore, the diffusion rate between mesopore and micropores was different. As shown in Figure 7, in the first linear sections of the dense film samples, the dye adsorptions reached 60–70% of the equilibrium after 200–300 min. However, for the fiber samples, about 95–97% dye was taken up in the first section within 20 min. The diffusion rate parameters ($k_{i,1}$; the slope of the first straight portion) of F10 were 2.5–11.6 times higher than those of the dense film. Because the adsorption occurring in the first section was relative to the most readily available sites on the sample surfaces, this revealed that the electrospun fibers

Table IV. Intraparticle Diffusion Parameters

		C_0 (mg/L)	$k_{i,1}$	R^2	$k_{i,2}$	R^2
Solvent Blue 35	Dense film	10	0.45	0.98	0.06	0.99
		40	0.51	0.99	0.14	0.97
	F10	10	1.14	0.97	0.01	0.72
		40	3.36	0.99	0.03	0.92
Oil Red O	Dense film	10	0.48	0.99	0.10	0.95
		40	0.74	0.99	0.18	0.99
	F10	10	3.54	0.99	0.04	0.69
		40	8.63	0.98	0.07	0.74

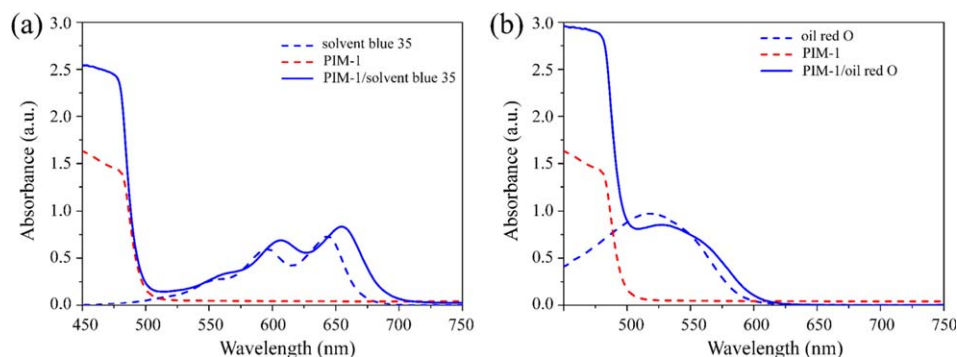$k_{i,2}$, the slope of the second straight portion.

Figure 8. UV–vis absorption spectra of the PIM-1 films before and after the adsorption of Oil Red O and Solvent Blue 35, Oil Red O, and Solvent Blue 35 in an ethanol solution. [Color figure can be viewed in the online issue, which is available at wileyonlinelibrary.com.]

possessed more mesopores, which were easier for the adsorbates to approach.[51] This result was also consistent with the observed higher surface area and the greater number of mesopores of the fiber samples by the BET surface area analysis. According to Table IV, the intraparticle rate parameters increased with initial dye concentrations. This was because the driving forces of the adsorption process increased with the dye concentration.

In the second linear sections, the diffusion rate parameters of the fiber samples were lower than those of the dense film samples. This may have been because of the fact that adsorption on the fiber samples almost reached equilibrium in the first section so that the driving force of the diffusion of the dye molecules was low. Although the rate parameters of the second sections of the dense film samples were higher, the thickness of the dense films was 50 μm; this was much higher than the diameters of the fiber samples (2 μm), and the total adsorption amount in the second sections of the dense film samples were about 30–40% of the equilibrium. It required more time for the diffusion of more dye molecules though the longer distance of the dense film samples. Therefore, it took 5000–6000 min for the adsorption processes on the film samples to reach equilibrium.

Host–Guest Interaction. Figure 8(a) shows the UV–vis spectra of the pristine PIM-1 film, Solvent Blue 35, and the PIM-1 film after absorbing Solvent Blue 35. Figure 8(b) shows the UV–vis spectra of the pristine PIM-1 film, Oil Red O, and the PIM-1 film after absorbing Oil Red O. As we observed, when the PIM-1 films were immersed in different dye solutions, they exhibited different extents of redshifts. Compared with the molecular structures of the dyes, PIM-1 could be considered an electron-deficient molecule. When PIM-1 contacted the dyes, charge-transfer interactions could occur between π-electron-rich (donor) molecules and π-electron-deficient (acceptor) molecules.[52,53] The PIM-1 films displayed a significant charge-transfer band from 500 to 520 nm in Figure 8(b), whereas no apparent charge-transfer band is shown in Figure 8(a). This result was consistent with the higher π-electron density of the Oil Red O compared to that of Solvent Blue 35. In addition, the redshifts in the UV–vis spectra of the two dyes were also observed. Therefore, the adsorption mechanism was a π–π electron donor–acceptor interactions between the electron-poor PIM-1 and electron-rich dyes. Furthermore, the greater charge-transfer interactions between the PIM-1 and Oil Red O resulted

in a higher adsorption amount of it than Solvent Blue 35, although the size and molecular weight of the former were greater than the latter.

For practical applications, adsorbent recycling shall also be considered. Through a variety of solvents tests, toluene and benzene had the abilities to regenerate the spent PIM-1 adsorbent. Because of the lower toxicity of toluene, we selected toluene as the regenerant. The reasons that toluene could regenerate the PIM-1 adsorbent were as follows: (1) first, the solubilities of the dyes were higher in toluene than in ethanol, and (2) toluene, as an aromatic compound, had a higher π-electron density than the dyes. Therefore, there was an adsorption competition between the dye and toluene to PIM-1, and the stronger charge-transfer interactions between the toluene and PIM-1 made the toluene molecules replace the dye molecules adsorbed on the PIM-1 surface.

CONCLUSIONS

In this study, we successfully fabricated smooth and uniform PIM-1 fibers. The PIM-1 fibers had more surface areas than the PIM-1 powder; this resulted from their higher intrafiber pores formed by fast evaporation of the solvent in the electrospinning process. Furthermore, the fibers had more mesopores so that the adsorption rates of the dyes on the fibers were much higher than those of the dense films. The dye adsorption data fit perfectly with the pseudo-second-order model and intraparticle model. The UV–vis analysis indicated that the adsorption mechanism between the dyes and PIM-1 was π–π interaction. Therefore, the dyes were desorbed from the PIM-1 fibers in toluene, which was a richer π-electron donor than the dye. Above all, the greater mesoporous PIM-1 fibers with superior adsorption performance have provided a new platform for the decontamination of organic solvents.

ACKNOWLEDGMENTS

REFERENCES

1. Smallwood, I. M. Solvent Recovery Handbook; CRC: Boca Raton, FL, **2002**.

2. Xing, D. Y.; Chan, S. Y.; Chung, T.-S. *Green Chem.* **2014**, *16*, 1383.

3. Wade, N. M. *Desalination* **2001**, *136*, 3.

4. Marchetti, P.; Jimenez Solomon, M. F.; Szekely, G.; Livingston, A. G. *Chem. Rev.* **2014**, *114*, 10735.

5. Szekely, G.; Jimenez-Solomon, M. F.; Marchetti, P.; Kim, J. F.; Livingston, A. G. *Green Chem.* **2014**, *16*, 4440.

6. Shao, L.; Cheng, X.; Wang, Z.; Ma, J.; Guo, Z. *J. Membr. Sci.* **2014**, *452*, 82.

7. Xu, Y. C.; Cheng, X. Q.; Long, J.; Shao, L. *J. Membr. Sci.* **2016**, *497*, 77.

8. Gorgojo, P.; Karan, S.; Wong, H. C.; Jimenez-Solomon, M. F.; Cabral, J. T.; Livingston, A. G. *Adv. Funct. Mater.* **2014**, *24*, 4729.

9. Fritsch, D.; Merten, P.; Heinrich, K.; Lazar, M.; Priske, M. *J. Membr. Sci.* **2012**, *401*, 222.

10. Volkov, A.; Stamatialis, D.; Khotimsky, V.; Volkov, V.; Wessling, M.; Plate, N. *J. Membr. Sci.* **2006**, *281*, 351.

11. Tsarkov, S.; Khotimskiy, V.; Budd, P. M.; Volkov, V.; Kukushkina, J.; Volkov, A. *J. Membr. Sci.* **2012**, *423*, 65.

12. Volkov, A.; Yushkin, A.; Kachula, Y.; Khotimsky, V.; Volkov, V. *Sep. Purif. Technol.* **2014**, *124*, 43.

13. Volkov, A.; Tsarkov, S.; Gokzhaev, M.; Bondarenko, G.; Legkov, S.; Kukushkina, Y. A.; Volkov, V. *Petrol. Chem.* **2012**, *52*, 598.

14. Hunger, K. Industrial Dyes: Chemistry, Properties, Applications; Wiley: Hoboken, NJ, **2007**.

15. Kim, J. F.; Szekely, G.; Schaepertoens, M.; Valtcheva, I. B.; Jimenez-Solomon, M. F.; Livingston, A. G. *ACS Sustain. Chem. Eng.* **2014**, *2*, 2371.

16. Yagub, M. T.; Sen, T. K.; Afroze, S.; Ang, H. M. *Adv. Colloid Interface Sci.* **2014**, *209*, 172.

17. Budd, P. M.; Elabas, E. S.; Ghanem, B. S.; Makhseed, S.; McKeown, N. B.; Msayib, K. J.; Tattershall, C. E.; Wang, D. *Adv. Mater.* **2004**, *16*, 456.

18. Doshi, J.; Reneker, D. H. In Conference Record of the 1993 IEEE Industry Applications Society Annual Meeting; Institute of Electrical and Electronics Engineers: NY, USA. **1993**; p 1698.

19. Lu, W.; Sun, J.; Jiang, X. *J. Mater. Chem. B* **2014**, *2*, 2369.

20. Dhandayuthapani, B.; Mallampati, R.; Sriramulu, D.; Dsouza, R. F.; Valiyaveettil, S. *ACS Sustain. Chem. Eng.* **2014**, *2*, 1014.

21. Zhang, C.; Li, P.; Cao, B. *Ind. Eng. Chem. Res.* **2015**, *54*, 8772.

22. Li, P.; Chung, T. S.; Paul, D. R. *J. Membr. Sci.* **2013**, *432*, 50.

23. Rüttermann, S.; Krüger, S.; Raab, W. H.-M.; Janda, R. *J. Dent.* **2007**, *35*, 806.

24. Taylor, G. P. *Proc. R. Soc. London Ser. A* **1969**, *313*, 453.

25. Theron, S.; Zussman, E.; Yarin, A. *Polymer* **2004**, *45*, 2017.

26. Gupta, P.; Elkins, C.; Long, T. E.; Wilkes, G. L. *Polymer* **2005**, *46*, 4799.

27. Geng, X.; Kwon, O.-H.; Jang, J. *Biomaterials* **2005**, *26*, 5427.

28. Bonso, J. S.; Kalaw, G. D.; Ferraris, J. P. *J. Mater. Chem. A* **2014**, *2*, 418.

29. Song, Q.; Cao, S.; Pritchard, R. H.; Ghalei, B.; Al-Muhtaseb, S. A.; Terentjev, E. M.; Cheetham, A. K.; Sivaniah, E. *Nat. Commun.* **2014**, 5. doi: 10.1038/ncomms5813

30. Weber, J.; Du, N.; Guiver, M. D. *Macromolecules* **2011**, *44*, 1763.

31. McDonald, T. O.; Akhtar, R.; Lau, C. H.; Ratvijitvech, T.; Cheng, G.; Clowes, R.; Adams, D. J.; Hasell, T.; Cooper, A. I. *J. Mater. Chem. A* **2015**, *3*, 4855.

32. Feng, L.-J.; Chen, Q.; Zhu, J.-H.; Liu, D.-P.; Zhao, Y.-C.; Han, B.-H. *Polym. Chem.* **2014**, *5*, 3081.

33. McKeown, N. B.; Budd, P. M. *Chem. Soc. Rev.* **2006**, *35*, 675.

34. Zhou, C.; Lee, S.; Dooley, K.; Wu, Q. *J. Hazard. Mater.* **2013**, *263*, 334.

35. Lin, J.; Ding, B.; Yang, J.; Yu, J.; Sun, G. *Nanoscale* **2011**, *4*, 176.

36. Heuchel, M.; Fritsch, D.; Budd, P. M.; McKeown, N. B.; Hofmann, D. *J. Membr. Sci.* **2008**, *318*, 84.

37. Shenoy, S. L.; Bates, W. D.; Frisch, H. L.; Wnek, G. E. *Polymer* **2005**, *46*, 3372.

38. Jeromenok, J.; Weber, J. *Langmuir* **2013**, *29*, 12982.

39. Gupta, V. *J. Environ. Manage.* **2009**, *90*, 2313.

40. Zur, L. S. *Sven. Vetenskapsakad. Handl.* **1898**, *24*, 1.

41. Ho, Y.-S.; McKay, G. *Chem. Eng. J.* **1998**, *70*, 115.

42. Kannan, N.; Sundaram, M. M. *Dyes Pigments* **2001**, *51*, 25.

43. Doan, M.; Zdemir, Y.; Alkan, M. *Dyes Pigments* **2007**, *75*, 701.

44. McKay, G. *Chem. Eng. J.* **1983**, *27*, 187.

45. Weber, W. J.; Morris, J. C. *J. Sanit. Eng. Div.* **1963**, *89*, 31.

46. Ho, Y.-S.; McKay, G. *Process. Biochem.* **2003**, *38*, 1047.

47. Sun, Q.; Yang, L. *Water Res.* **2003**, *37*, 1535.

48. Allen, S.; Mckay, G.; Khader, K. *Environ. Pollut.* **1989**, *56*, 39.

49. Simons, G. A. In Symposium (International) on Combustion, Elsevier: Netherlands **1982**; p 1067.

50. Simons, G. A. *Combust. Flame* **1983**, *50*, 275.

51. Hsieh, C.-T.; Teng, H. *Carbon* **2000**, *38*, 863.

52. Chen, J.; Chen, W.; Zhu, D. *Environ. Sci. Technol.* **2008**, *42*, 7225.

53. Zhu, D.; Pignatello, J. *J. Environ. Sci. Technol.* **2005**, *39*, 2033.